Measurement of the separation dependence of resonant energy transfer between CdSe/ZnS core/shell nanocrystallite quantum dots

Farbod Shafiei, Sannah P. Ziama, Eric D. Curtis, and Ricardo S. Decca*
Department of Physics, Indiana University-Purdue University Indianapolis, Indianapolis, Indiana 46202, USA
(Received 9 May 2010; revised manuscript received 31 March 2011; published 1 August 2011)

The separation dependence of the interaction between two resonant groups of CdSe/ZnS nanocrystallite quantum dots is studied at room temperature. A near-field scanning optical microscope is used to bring a group of monodisperse ∼6.5-nm-diam nanocrystallite quantum dots, which are attached to the microscope probe, into close proximity of an ∼8.5-nm-diam group of nanocrystallite quantum dots which are deposited on a solid immersion lens. Information extracted from photoluminescence, photoluminescence excitation, and absorption curves as well as numerical calculations of the energy levels show that the third excited excitonic energy level of the large quantum dots nearly matches the ground excitonic energy level for the small quantum dots. Quenching of the small quantum dots' photoluminescence signal is observed as they approach the large quantum dots. On average, the separation between microscope probe and solid immersion lens changed in the 15–50-nm range. The transition probability between these two groups of quantum dots is calculated to be $(2.60 \times 10^{-47}\ \mathrm{m}^6)/R^6$, within the experimentally obtained range of transition probabilities $(0.70 \times 10^{-47}\ \mathrm{m}^6)/R^6$–$(11.0 \times 10^{-47}\ \mathrm{m}^6)/R^6$. The Förster radius, as a signature of energy transfer efficiency, is experimentally found to be in the 14–22-nm range.

DOI: 10.1103/PhysRevB.84.075301 PACS number(s): 78.67.Hc, 78.66.Hf, 07.79.Fc

I. INTRODUCTION

Advancements in semiconductor technology, starting in late 1980s, allowed for the fabrication of nanocrystallite quantum dots (NQDs), consisting of a few hundred to many thousand atoms[1] of semiconductor materials producing a potential well for electrons and holes. NQDs are fabricated such that their diameters are smaller than the bulk Bohr exciton diameter; thus, the electronic structure is dominated by quantum confinement effects in all three dimensions[2–4] and is suited for the study of zero-dimensional structures.[1,5,6] Colloidal NQDs, which are synthesized by relatively inexpensive wet chemistry methods, have high control in engineering the energy levels. This results in NQDs with strong size-dependent optical and electrical properties.[1] In particular, CdSe NQDs can be synthesized with a tunable size of 15–100 Å in a narrow distribution (<5% rms dispersion).[7]

The emission properties of NQDs are often measured via photoluminescence (PL) experiments. In PL, excitonic states in the semiconductor material are induced by photon absorption, and the optical emission as these excitons recombine is analyzed. In Förster resonant energy transfer (FRET), an excited donor can transfer its energy directly (nonradiatively) to an acceptor via dipole-dipole interaction. The phenomenon of resonant energy transfer was observed by Perrin[8,9] at the beginning of the 20th century, but it was Förster in the late 1940s[10] who proposed a theory describing long-range molecular interaction by resonance energy transfer. Due to its strong separation dependence, FRET has been used as a molecular ruler to determine inter- and intramolecular distances.[11] Since FRET represents a transfer of energy, it can be detected by measuring the quenching of donor emission or the enhancement of acceptor emission. This relationship of the transfer rate as a function of donor-acceptor separation was first demonstrated with peptides in 1963.[12]

Controlling the distance between the NQDs in real time has been a challenge faced by most groups studying the dynamic process of energy transfer between NQDs.[13–22] We use a near-field scanning optical microscope (NSOM) to control the distance between two groups of NQDs in real time. In this experiment a group of core/shell CdSe/ZnS NQDs with an external diameter of ∼6.5 nm, attached to the apex of the NSOM probe, is brought into close proximity to a second group of CdSe/ZnS NQDs with an external diameter of ∼8.5 nm, which are deposited on the flat part of a solid immersion lens (SIL). Both groups of NQDs are excited and the PL signal of the small NQDs is monitored to observe any changes. Using an Al-coated NSOM probe and diluting the NQDs helps to reduce the number of NQDs excited on the NSOM probe and SIL.

II. EXPERIMENT

A. Experimental setup

An aperture NSOM has been designed and built to be used as a probe to excite a small number of CdSe/ZnS core/shell NQDs. There were two primary reasons for using a NSOM system. The first was to overcome the diffraction limit[23–28] arising from far-field microscopy, and the second was to gain precise and direct control over the relative positioning of distinct groups of NQDs.[23–29] Small NQDs are attached to the apex of a NSOM probe by dipping the probe into the colloidal suspension of the NQDs, while large NQDs are diluted and deposited on the SIL by drop cast. All NQDs are covered by octadecylamine (ODA) ligands. The inset of Fig. 1 schematically shows the probe's Al coating precluding the excitation of the NQDs outside its apex.

As shown in Fig. 1, the probe's vertical motion is controlled by a feedback loop system while its lateral motion is computer controlled. The amplified signal from the feedback loop system and the computer are applied to a three-axis piezo stage. The NSOM probe is assembled on a tripod which sits on the piezo stage. The probe approaches the flat side of a SIL through a hole on the SIL holder. While all the results reported in this paper were obtained at room temperature, the SIL holder

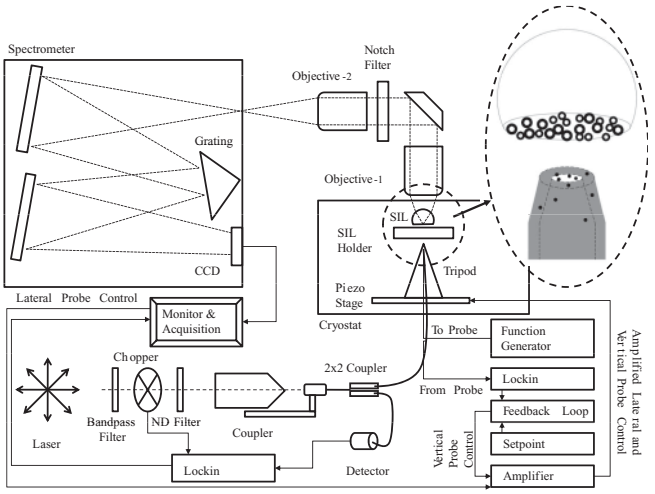

FIG. 1. Schematic of experimental setup including NSOM. Inset: Schematic of NSOM probe and SIL (not to scale) with small NQDs on the NSOM probe and large ones on the SIL. Distance between small and large NQDs changes by moving the NSOM probe toward and away from the SIL. PL signals of both groups of NQDs are collected on the CCD camera in the spectrometer.

also serves the purpose of cooling down the SIL because it is in thermal contact with the cryostat's cold finger. An argon laser (488-nm line) has been used for optical excitation. To improve on the signal-to-noise ratio of the monitored signal, the laser light is chopped before being coupled into a single-mode optical fiber. The use of the 2×2 fiber splitter, a Si photodiode, and standard lock-in detection allows for continuous monitoring of the laser intensity coupled to the NSOM probe. After excitation of small and large NQDs on the NSOM probe and the SIL, photons released by these two groups of NQDs are collected through the SIL and two other objectives. They are then dispersed by a grating spectrometer and their energy is recorded on a charge-coupled device (CCD).

B. Measurement of the distance between small and large NQDs

In the NSOM system, the amplitude of vibration of the NSOM probe, glued to a vibrating tuning fork driven at resonance, has been used as an input for the feedback loop circuit.[29] This circuit controls the distance between the NSOM probe and the SIL. The vibrational amplitude of the NSOM probe decreases as it is driven toward the SIL.[29–32] This amplitude damping has been used to measure the probe-SIL separation. To be able to measure this distance, the probe is engaged in close proximity of the SIL and then moved toward the SIL by decreasing the set point in the feedback loop system. As the probe approaches the SIL and its amplitude decreases, the system reaches the point when it becomes unstable and the probe would break if it is moved any further. This point is assumed to be the contact point between the NSOM probe and the SIL. The separation is then increased by pulling back the probe by increasing the set point. Since the voltage applied to move the probe away from contact, as well as the displacement calibration of the piezo stage as a function of voltage, are known, the separation between the NSOM probe and the SIL can be obtained. Hence, in other experiments the voltage-separation calibration curve has been used to identify the distance between the small and large NQDs that are on the NSOM probe and the SIL, respectively.

C. Resonant CdSe/ZnS NQDs

Specific sizes of small and large NQDs are selected to have the excitonic ground state of the small CdSe/ZnS NQDs coincide with one of the excited states of the large CdSe/ZnS NQDs. This energy selection is accomplished by a numerical calculation of the energy levels, and verified by PL, photoluminescence excitation (PLE), and absorption experiments. PL measurements were used to study the energy structure of the NQDs by using the photon excitation and relaxation. It is shown in the theory section that when the PL signal of the large NQDs with ~8.5 nm diameter is observed at ~630 nm, the calculated corresponding PL signal for the resonant set of small NQDs should be at ~570 nm, which corresponds to NQDs with ~6.5 nm diameter. The vertical lines in Fig. 2 show the calculated third excited and ground-state energy levels of large NQDs at 567 and 631 nm. To find a resonant pair of NQDs, PL signals of various NQDs have been studied. As shown in Fig. 2 by the absorbance spectrum for the large NQDs (provided by the NQDs distributer, N. N. Labs LLC), there is an energy level at ~570 nm for the large NQDs with a ground-state energy level at ~630 nm. This was confirmed by PLE experiments. The PLE graph, which is similar to the absorption graph, shows a strong absorption at ~570 nm with emission at ~630 nm.

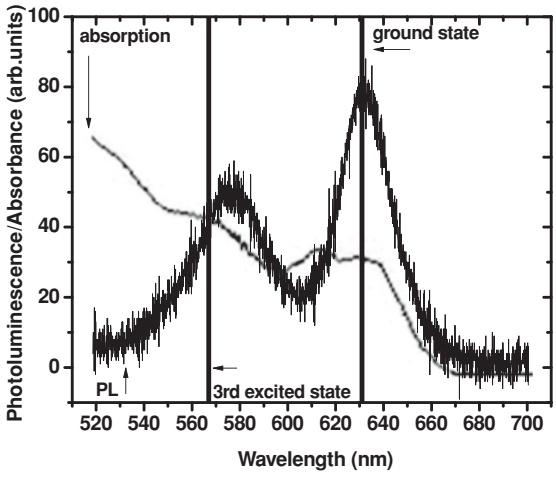

FIG. 2. Comparison of calculated energy levels, the absorbance spectrum of large NQDs, and PL of resonant NQDs. Vertical lines at 567 and 631 nm show numerically calculated third excited and ground-state energy levels of large CdSe/ZnS NQDs with ~8.5 nm diameter. The fine line shows the absorbance spectrum of large CdSe/ZnS NQDs provided by N.N. Labs LLC. This absorbance spectrum shows that the large NQDs with -nm ground-state energy have an excited energy level also at 570 nm. PL signals from small NQDs on the NSOM probe and large NQDs on the SIL excited by an argon laser (488 nm) are shown as a thick line. The calculated third excited energy level and absorption spectrum of large NQDs at 570 nm matches the PL signal of the small NQDs.

D. Resonant energy transfer between CdSe/ZnS NQDs as a function of separation

Energy-matched NQDs are used for the resonant energy transfer experiments. The area of the PL signal of small NQDs is monitored for any change. The small NQDs on the NSOM probe are optically excited, and the induced excitons relax to their ground state, recombining and releasing a photon. These photons are collected through the SIL and sent to a spectrometer generating the high-energy peak of the spectrum in Fig. 2. This same process also occurs with the large NQDs, generating the low-energy peak of the spectrum in Fig. 2. As NQDs are brought into close proximity, a portion of energy would be expected to non-radiatively transfer from the small NQD to the large NQD. This interaction, associated to the nonradiative energy transfer from the ground state of the small NQDs to the third excited state of the large NQDs, becomes increasingly more important as the separation between the NSOM probe and the SIL decreases,[10] within the near-field region. Furthermore, since the intradot relaxation time is very fast,[33–36] in the subpicosecond to picosecond range, energy transfer from the large NQDs to the small ones is precluded.

The separation-induced quenching of the small-NQDs signal is a clear signature of the interaction between two groups of resonant NQDs. Quenching of the small NQDs PL signal is shown in Fig. 3. The small-NQDs PL signal decreases as a function of separation: the area under the PL signal decreases in the 15 286, 15 026, 14 846, 14 740, 14 496, 14 352, and 14 006 sequence for corresponding separations of 37, 35, 32, 30, 27, 23, and 18 nm, respectively. Each PL spectrum in this experiment was integrated over 120 s.

The corresponding enhancement in the large-NQDs PL signal was not observed as the number of NQDs on the SIL was not under control. As a consequence of the deposition process of the large NQDs on the SIL, many NQDs agglomerate.

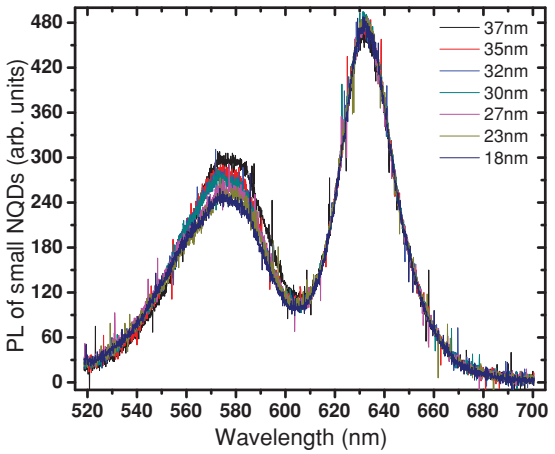

FIG. 3. (Color online) PL signal of small and large NQDs as a function of separation between the NSOM probe and the SIL. The PL signal of small NQDs decreases as the separation between the two groups of NQDs decreases. The PL signal of small NQDs at the left side from top to bottom corresponds to 37, 35, 32, 30, 27, 23, and 18 nm separation between the NSOM probe and the SIL. An enhancement of the large-NQDs PL signal was not observed as a consequence of the deposition process of the large NQDs on the SIL (see Fig. 4).

Lowering the concentration of large NQDs on the 2.5-mm-wide SIL did not prevent their agglomeration. This packed ensemble of monodispersed large NQDs allows energy transfer between similar-sized neighboring *large* NQDs, beyond the area above the NSOM probe. Hence, numerous large NQDs get excited, as observed in the spectrometer images. The spectrometer images in Fig. 4 show that large NQDs are excited beyond the area above the NSOM probe, strongly suggesting that neighboring NQDs transfer energy to each other. Consequently, the area under the PL signal of large NQDs is mostly constant.

Figure 5 shows the reduction of the PL signal of the small NQDs as a function of separation between the NSOM probe and the SIL. In this figure the area under the PL signal of small NQDs has been normalized to the area of the large-NQDs PL signal. This last normalization process is undertaken to cancel out small fluctuations associated with the laser intensity. As shown in the figure, when the separation reaches ∼20 nm, the decrease in PL signal from the small NQDs stops, which is believed to be the contact point between the two groups of NQDs on the NSOM probe and the SIL. After this separation the PL signal of the small NQDs remains constant. The difference between this contact point and the sum of the diameters of the two NQDs (∼15 nm) could be partially due to the existence of 2.5-nm-long and tightly bounded ODA ligands on the outer shell of the NQDs which prevent full contact of the NQDs.[37,38] This separation is interpreted as a zero of the FRET spectroscopic ruler.

The experiment was also done with a SIL which had no NQDs deposited upon its surface, while maintaining the small NQDs on the probe. The PL signal of the small NQDs does not change as the probe approaches the clean SIL, as it is shown by the square symbols in Fig. 6. On the other hand, the triangles in Fig. 6 show the quenching of the small-NQDs PL signal when both groups of small and large resonant NQDs are present. To further enhance the argument that the change of PL signal in small NQDs is due to FRET, nonresonant small and large NQDs were brought close together. No quenching in the small-NQDs PL signal is observed, as shown by the circles in Fig. 6. Small-sized NQDs were chosen to have a different ground-state energy level than any levels of the large NQDs.

III. THEORY

A. Energy levels of the CdSe/ZnS

Single band effective mass approximation[39–41] was used to study the excitonic energy levels of NQDs. This process helped us choose the right resonant NQDs for the experiment. This numerical calculation showed us that a large CdSe/ZnS with core radius of 3.7 nm and shell radius of 4.25 nm with ground-state energy level of 3.135×10^{-19} J (631 nm) has its third excited energy level at 3.486×10^{-19} J (567 nm). This makes it resonant with a small CdSe/ZnS with outer radius of 3.25 nm with a ground-state energy-level emission at 570 nm. The presence of ODA ligands on NQDs does not change the energy levels.

The analysis is first restricted to the strong confinement regime, where the Coulomb interaction between particles is neglected in comparison to the confinement energy. At

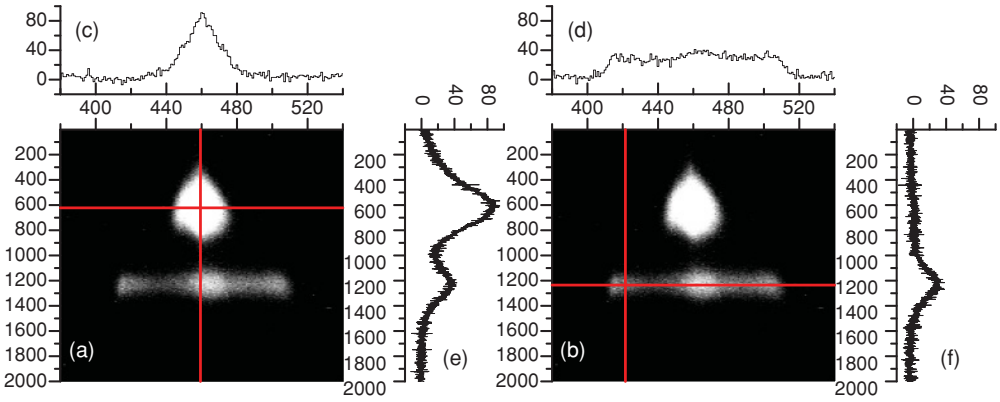

FIG. 4. (Color online) (a, b) Images of small NQDs on the NSOM probe and large NQDs on the SIL are collected by the spectrometer. These images show the distribution of photons as a function of energy on vertical axes. The horizontal axes show the spatial distribution of NQDs. All axes are labeled by their pixel number. (c–f) Horizontal and vertical cross cuts from images (a) and (b) are shown on the top and right-hand side of each image. (c) Horizontal cross cut of image (a) shows that small NQDs are clearly confined to the NSOM probe apex area (around pixel number 600). (d) Horizontal cross cut of image (b) shows that large NQDs are excited beyond the excitation area of the NSOM probe on the SIL (around pixel number 1200). (e, f) Vertical cross cuts show the spectrum as a function of energy.

the core/shell boundary ($r = r_c$) the continuity of the wave function and the probability current,[42,43] as well as the boundary condition on the wave function at the shell/vacuum boundary of the NQDs (assumed to be immersed in vacuum), yields the energy levels of the free particles (electrons and holes). The shell radius of the NQDs, r_s, is obtained from small-angle x-ray diffraction scattering. Knowing r_s, the core radius r_c can be adjusted to change the ground-state energy level of the calculation, which is then used to find other energy levels.

Later the electron-hole Coulomb interaction energy is considered as a correction to the total Hamiltonian. This last term is small and is treated as a heliumlike perturbation[41] for the electron and hole energy of the system. At this point, by adjusting r_c, the ground-state energy due to strong confinement and electron-hole Coulomb interaction correction can be calculated and compared to the observed PL peak of the NQDs. Matching the calculated energy of the ground state and the observed PL peak leads us to choose the right r_c. For $r_c = 3.7$ nm and $r_s = 4.25$ nm, the first four energy levels and their Coulomb correction are shown in Table I. The calculated excited energy levels are compared to the absorption peaks of the NQDs showing very good agreement.

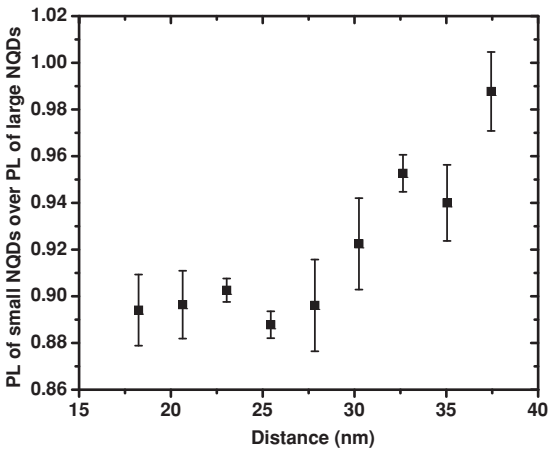

FIG. 5. Area under the small NQDs PL signal as a function of separation between the NSOM probe and the SIL. These areas have been normalized by the large-NQDs signal areas. The experiment was repeated five times for each point and the standard errors are used to calculate the error bars.

B. Dipole-dipole interaction and resonant energy transfer

The energy of any charge distribution in the presence of other charge distributions and external electrical potential can be obtained by a multipolar expansion.[47] Since both NQDs

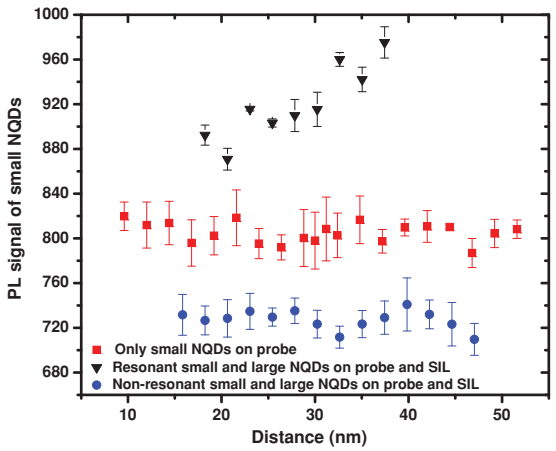

FIG. 6. (Color online) PL signals of small NQDs interacting with resonant large NQDs (triangles, data shifted for clarity) show quenching as the NSOM probe approaches the SIL. PL signals of small NQDs when there are no large NQDs on the SIL (squares) do not show any changes as the NSOM probe approaches the SIL. PL signals of small NQDs in the presence of nonresonant large NQDs do not show any changes (circles, data shifted for clarity). All PL signals have been normalized to laser intensity. Each experiment was repeated five times for each separation and the standard errors are used to calculate the error bars.

TABLE I. Table of calculated confinement energy levels and Coulomb correction terms for CdSe/ZnS NQDs with $r_c = 3.7$ nm and $r_s = 4.25$ nm. ℓ_e and ℓ_h are quantum numbers of electrons and holes inside the NQDs. The last column is the calculated wavelength for the excitonic recombination. In addition to effective masses and band gap, the conduction bands offset between CdSe and ZnS were used for these calculations.[44–46]

ℓ_e	ℓ_h	E_e (J)	E_h (J)	E_c (J)	E_{tot} (J)	λ (nm)
0	0	1.699×10^{-19}	1.554×10^{-19}	-1.22×10^{-20}	3.135×10^{-19}	631
0	1	1.699×10^{-19}	1.643×10^{-19}	-1.13×10^{-20}	3.233×10^{-19}	612
1	0	1.943×10^{-19}	1.554×10^{-19}	-1.17×10^{-20}	3.384×10^{-19}	584
1	1	1.943×10^{-19}	1.643×10^{-19}	-9.60×10^{-21}	3.486×10^{-19}	567

are neutral, the first term which survives is the dipole-dipole interaction energy, due to the dipolar electric field of one of the excitons interacting with the other NQDs exciton's dipole.

This energy of interaction between electric multipoles may be found by expanding the Coulomb interaction. First consider two charge distributions, 1 and 2, centered at O_1 and O_2, respectively, with coordinate axes chosen to be parallel. The distance between these two origins is defined as R, which makes an angle θ with the z axis of the first charge distribution. The separation between two elements, i and j, of these two charge distributions is defined as r_{ij}. By expanding this distance into spherical harmonics, the electrostatic interaction can be written as[48,49]

$$V_{12} = \sum_{i,j}\left(\frac{e^2}{r_{ij}}\right) = \frac{1}{4\pi\epsilon}e^2\sum_{i,j}\sum_{\ell,\ell'}\frac{(-1)^{\ell'}r_i^{\ell}r_j^{\ell'}}{R^{\ell+\ell'+1}} \times \sum_{m,m'} B_{\ell\ell'}^{mm'}Y_{\ell+\ell'}^{-m-m'}(\theta,0)Y_{\ell}^{m}(\theta_i,\phi_i)Y_{\ell'}^{m'}(\theta_j,\phi_j), \quad (1)$$

where

$$B_{\ell\ell'}^{mm'} = \frac{(-1)^{m+m'}(4\pi)^{\frac{3}{2}}}{[(2\ell+1)(2\ell'+1)(2\ell+2\ell'+1)]^{\frac{1}{2}}} \times \left(\frac{(\ell+\ell'+m+m')!(\ell+\ell'-m-m')!}{(\ell+m)!(\ell-m)!(\ell'+m')!(\ell'-m')!}\right)^{\frac{1}{2}}. \quad (2)$$

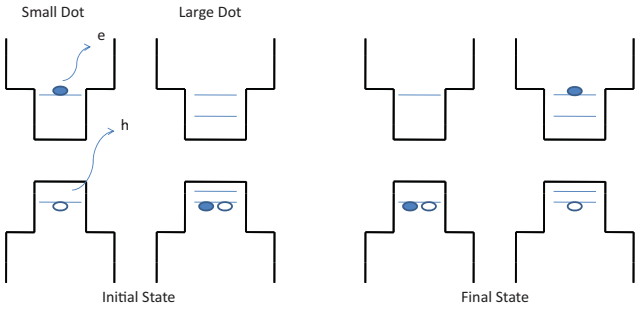

FIG. 7. (Color online) Initial and final states of combination of small and large NQDs before and after the energy transfer. In the initial state, the small-NQD exciton is in its ground state and no exciton exists in the large NQD. In the final state, there is no exciton in the small NQD and the large-NQD exciton is in its third excited state.

For the case of interaction between two NQDs, i is the charge distribution of the first NQD and j belongs to the second NQD. When the ground state of the small NQD ($\ell_e = 0, \ell_h = 0$) is in resonance with the third excited state of the large NQD ($\ell_e = 1, \ell_h = 1$), the emission peak of the small NQD overlaps with the fourth absorption peak of the large NQD. Both of these states are optically active due to the p symmetry in the valence band.

We have used Eqs. (1) and (2) to calculate the transition rate $W = \frac{2\pi}{\hbar}|\langle V_{12}\rangle|^2\rho$,[50–54] where $\langle V_{12}\rangle$ is the Coulomb potential energy between the small and large NQDs and ρ is the normalized overlap between donor emission and acceptor absorption spectra.[50–53] From this equation, the transition probabilities $P = W\tau$ are obtained, where τ represents the donor's lifetime. Since the exciton at the ground state on the small NQDs recombines after τ, the energy transfer between two resonant NQDs happens in times shorter than τ. The overall initial wave function is the product of the wave function of the exciton (electron-hole pair) at its ground state in the small NQD and the wave function of no exciton in the large NQD (which is equivalent to having an electron and hole both in the first excited energy level in the valence band of the large NQD). Similarly the overall final wave function is considered to be the product of the wave function of no exciton in the small NQD and the wave function of an exciton at the third excited energy state in the large NQD. Figure 7 shows the initial and final states considered. Using these initial and final states, $\langle V_{12}\rangle = \frac{1.19\times10^{-46}}{r^3}$ Jm^3 is obtained. Here the normalized overlap between donor's emission and acceptor's absorption, $\rho = 3.09 \times 10^{19}$, obtained from the experimental data, has been used. Hence, the transition rate is $W = \frac{2\pi}{\hbar}\langle V_{12}\rangle^2\rho = (2.60 \times 10^{-38}\frac{\text{m}^6}{\text{s}})/r^6$ and the transition probability is $P = W\tau = (2.60 \times 10^{-47}\ \text{m}^6)/r^6$ by considering $\tau = 1$ ns. The radiative lifetime of CdSe or CdSe/ZnS has been measured or calculated to be in the range of a few nanoseconds up to several tens of nanoseconds.[35,55–62]

IV. DISCUSSION

Data similar to those reported in Fig. 3 have been used to derive the transition probability of the resonant energy transfer between these two groups of NQDs. The procedure to obtain the transition probability is given by

$$P = \frac{A(\infty) - A(r)}{A(\infty)}, \quad (3)$$

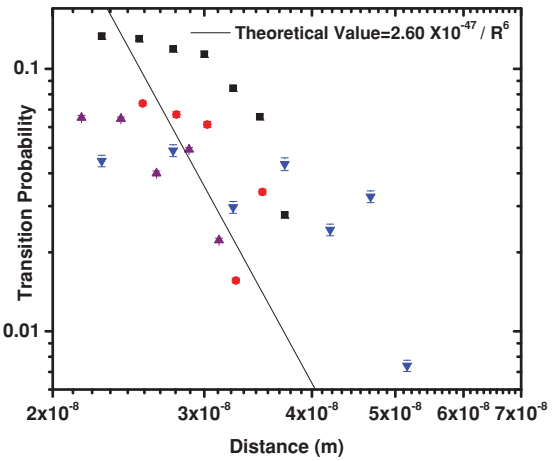

FIG. 8. (Color online) Transition probability from four different experiments and theoretical calculation as a function of separation. The vertical axis represents the transition probability, obtained by subtracting the normalized small-NQDs PL signal at the farthest experimental point from the normalized small-NQDs PL at the measurement point, divided by the normalized PL signal at the farthest distance. The solid line shows the theoretical value for the transition probability calculated in Sec. III B using a dipole-dipole approximation.

where $A(r)$ is the normalized area of the PL signal of the small NQDs at a separation r and $A(\infty)$ is the corresponding one at an infinite separation, when there is no interaction between the small and large NQDs. Equation (3) represents the fact that as the two groups of NQDs get closer the dipole-dipole interaction increases and the probability of resonant energy transfer increases. Hence, the normalized PL signal of the small NQDs decreases proportionally to the square of the strength of the interaction. In the experimental case $A(\infty)$ has been selected at the distance when the interaction is the smallest, i.e., the largest experimentally accessible separation between groups of NQDs. Since the PL signal of small NQDs cannot be collected when they are very far away from the SIL, a position where the PL signal from small NQDs is completely collected has to be used as a reference. Furthermore, the feedback interaction between the NSOM probe and the SIL happens over ~50 nm, which limits the point for the largest separation to about this value. As an example, for the experiment from which Fig. 5 was extracted, this distance is 37 nm.

Figure 8 shows the transition probability for four experimental sets. The theoretical value for the transition probability (2.60×10^{-47} m$^6/r^6$) is also shown in the figure.

The transition probability also provides the Förster radius as it is represented by R_o in the Förster rate equation.[10,63–65] By comparing $(R_o/r)^6$ from the Förster rate equation and its equivalent experimental transition probability, the Förster radius is calculated to be in the 14–22-nm range. From the theoretically calculated transition probability, the radius R_o is extracted to be 17 nm. A Förster radius of 4.7 nm was obtained by Kagan *et al.*[13,14] using differently sized CdSe NQDs and capping ligands, under a close-packed mixture of two sizes of NQDs. In our experiment the measurement is between small and large NQDs that are isolated from each other, whereas in Refs. 13 and 14 it is between mixed small and large NQDs. The authors of Refs. 13 and 14 used spectral overlap of the donor emission and acceptor absorption integral to measure the Förster radius. Kagan *et al.* show[13,14,66]

$$R_o^6 \propto \frac{\varphi_D}{n^4} \int_0^\infty F_D(\nu)\varepsilon_A(\nu)\frac{d\nu}{\nu^4}, \tag{4}$$

where ν is the frequency, φ_D is the donor luminescence quantum yield, and n is the effective index of refraction. $F_D(\nu)$ is the normalized spectrum for the donor and $\varepsilon_A(\nu)$ is the molar extinction coefficient for acceptor absorption. The authors used a random close-packed mixture of NQDs with organic caps filling interstices and considered the volume-weighted average of the index of refraction of CdSe ($n = 2.58$) and organic caps ($n = 1.47$) as an effective index of refraction. In our experiment, isolating small NQDs from large NQDs would make n smaller in comparison to these works because of the presence of air between the interacting NQDs. This screening effect has been discussed previously in similar systems.[67] Using n, spectral overlap and φ_D under our experimental conditions would bring the Förster radius obtained from Refs. 13 and 14 in close agreement with our data. By considering the parameters for Guo *et al.*'s work,[68] a similar conclusion can be obtained.

V. CONCLUSION

In conclusion, resonant energy transfer between two groups of CdSe/ZnS as a function of separation has been observed directly from the PL signal of small NQDs. Small CdSe/ZnS NQDs on the apex of the NSOM probe were brought into close proximity to the resonant large NQDs on the SIL and both groups of NQDs were optically excited. Because the third excited-state energy level of large NQDs is the closest energy level to the ground-state energy level of the small NQDs, some fraction of the energy was transferred from small NQDs to the large NQDs before recombination took place in the small NQDs. Figure 8 indicates that the interaction between resonant NQDs could be a dipole-dipole interaction. Within the experimental resolution, this energy transfer is compatible with a dipole active one and depends on distance as dipole-dipole interaction ($\propto \frac{1}{r^6}$). In the future, more work will be needed to isolate a single small NQD on the NSOM probe and a single large NQD on the SIL.

In all experiments, the small PL signal reaches a point where the quenching stops and the PL signal becomes constant, which seems to correspond to the contact point of the small and large NQDs as they get close enough to each other. For all of the experiments this contact point is ~20 nm, comparable to the sum of the size of the two NQD diameters of ~15 nm. This difference is mostly due to the presence of the 2.5-nm-long tightly bounded ODA ligands on the NQDs.

The experimental transition probability between ~6.5- and ~8.5-nm-diam CdSe/ZnS NQDs is measured in the range $(0.7 \times 10^{-47}$ m$^6)/r^6$–$(11.0 \times 10^{-47}$ m$^6)/r^6$, while the theoretically calculated value is $(2.60 \times 10^{-47}$ m$^6/r^6)$. More precise data are needed for obtaining a better fitting. Comparison of the Förster radius from our experiment, 14–22 nm, with the distance between NSOM probe and the SIL (15–50 nm),

shows that coupling between NQDs is a near-neighbor interaction.

ACKNOWLEDGMENTS

This work was supported in part by the National Science Foundation through Grants No. CCF-0508239 and No. PHY-0701636, and Los Alamos National Laboratory support through Contract No. 49423-001-07. The authors are also indebted to the Nanoscale Imaging Center at IUPUI for the liberal use of the installations. We are also indebted to Dr. Horia Petrache for conducting the NQD size measurement by small-angle x-ray scattering and to Cynthia Wassall for preparing the SIL.

*rdecca@iupui.edu

[1] A. P. Alivisatos, Science **271**, 933 (1996).
[2] L. Al. Efros and L. A. Efros, Sov. Phys. Semicond. **16**, 772 (1982).
[3] L. E. Brus, J. Chem. Phys. **80**, 4403 (1984).
[4] S. A. Reimann and Matti Mannien, Rev. Mod. Phys. **74**, 1283 (2002).
[5] L. Brus, Appl. Phys. A Mater. **53**, 465 (1991).
[6] S. A. Empedocles, D. J. Norris, and M. G. Bawendi, Phys. Rev. Lett. **77**, 3873 (1996).
[7] C. B. Murray, D. Norris, and M. G. Bawendi, J. Am. Chem. Soc. **115**, 8706 (1993).
[8] P. Wu and L. Brand, Anal. Biochem. **218**, 1 (1994).
[9] B. R. Masters and P. T. C. So, *Hand Book of Biomedical Nonlinear Optical Microscopy* (Oxford University Press, New York, 2008).
[10] V. T. Forster, Ann. Phys. **6**, 55 (1948).
[11] L. Stryer, Annu. Rev. Biochem. **47**, 819 (1978).
[12] H. Edelhoch, L. Brand, and M. Wilcheck, Isr. J. Chem. **1**, 216 (1963).
[13] C. R. Kagan, C. B. Murray, and M. G. Bawendi, Phys. Rev. B **54**, 8633 (1996).
[14] C. R. Kagan, C. B. Murray, M. Nirmal, and M. G. Bawendi, Phys. Rev. Lett. **76**, 1517 (1996).
[15] S. A. Crooker, J. A. Hollingsworth, S. Tretiak, and V. I. Klimov, Phys. Rev. Lett. **89**, 186802 (2002).
[16] W. Nomura, T. Yatsui, T. Kawazoe, and M. Ohtsu, J. Nanophotonics **1**, 011591 (2007).
[17] C. W. Chen, C. H. Wang, Y. F. Chen, C. W. Lai, and P. T. Chou, Appl. Phys. Lett. **92**, 051906 (2008).
[18] W. Lü, I. Umezu, and A. Sugimura, Jpn. J. Appl. Phys. **47**, 6592 (2008).
[19] D. G. Kim, S. Okahara, M. Nakayama, and Y. G. Shim, Phys. Rev. B **78**, 153301 (2008).
[20] D. G. Kim, K. Okazaki, and M. Nakayama, Phys. Rev. B **80**, 045322 (2009).
[21] C. H. Wang, C. W. Chen, Y. T. Chen, C. M. Wei, Y. F. Chen, C. W. Lai, M. L. Ho, P. T. Chou, and M. Hofmann, Appl. Phys. Lett. **96**, 071906 (2010).
[22] K. Tai, W. Lü, I. Umezu, and A. Sugimura, Appl. Phys. Express **3**, 035202 (2010).
[23] D. W. Pohl, W. Denk, and M. Lanz, Appl. Phys. Lett. **44**, 651 (1984).
[24] A. Harootunian, E. Betzig, M. Isaacson, and A. Lewis, Appl. Phys. Lett. **49**, 674 (1986).
[25] U. Dürig, D. W. Pohl, and F. Rohner, J. Appl. Phys. **59**, 3318 (1986).
[26] E. Betzig, M. Isaacson, and A. Lewis, Appl. Phys. Lett. **51**, 2088 (1987).
[27] E. Betzig, J. K. Truatman, T. D. Harris, J. S. Weiner, and R. L. Kostelak, Science **251**, 1468 (1991).
[28] E. Betzig and J. K. Trautman, Science **257**, 189 (1992).
[29] K. Karrai and R. D. Grober, Appl. Phys. Lett. **66**, 1842 (1995).
[30] E. Betzig, P. L. Finn, and J. S. Weiner, Appl. Phys. Lett. **60**, 2484 (1992).
[31] R. Toledo Crow, P. C. Yang, Y. Chen, and M. Vaez Iravani, Appl. Phys. Lett. **60**, 2957 (1992).
[32] R. D. Grober, T. D. Harris, J. K. Trautman, and E. Betzig, Rev. Sci. Instrum. **65**, 626 (1994).
[33] Al. L. Efros, V. A. Kharchenko, and M. Rosen, Solid State Commun. **93**, 281 (1995).
[34] P. Guyot-Sionnest and M. A. Hines, Appl. Phys. Lett. **72**, 686 (1998).
[35] V. I. Klimov, D. W. McBranch, C. A. Leatherdale, and M. G. Bawendi, Phys. Rev. B **60**, 13740 (1999).
[36] P. Guyot-Sionnest, B. Wehrenberg, and D. Yu, J. Chem. Phys. **123**, 074709 (2005).
[37] N. Belman, S. Acharya, O. Konovalov, A. Vorobiev, J. Israelachvili, S. Efrima, and Y. Golan, Nano Lett. **83**, 3858 (2008).
[38] J. J. Li, Y. A. Wang, W. Guo, J. C. Keay, T. D. Mishima, M. B. Johnson, and X. Peng, J. Am. Chem. Soc. **125**, 12567 (2003).
[39] A. R. Kortan, R. Hull, R. L. Opila, M. G. Bawendi, M. L. Steigerwald, P. J. Carol, and L. E. Brus, J. Am. Chem. Soc. **112**, 1327 (1990).
[40] J. W. Haus, H. S. Zhou, I. Honma, and H. Komiyama, Phys. Rev. B **47**, 1359 (1993).
[41] D. Schooss, A. Mews, A. Eychmuller, and H. Weller, Phys. Rev. B **49**, 17072 (1994).
[42] D. J. Ben Daniel and C. B. Duke, Phys. Rev. **152**, 683 (1968).
[43] L. E. Brus, J. Chem. Phys. **79**, 5566 (1983).
[44] J. C. Miklosz and R. G. Wheeler, Phys. Rev. **153**, 913 (1967).
[45] J. O. Dimmock and R. G. Wheeler, J. Appl. Phys. **32**, 2271 (1961).
[46] A. N. Nethercot, Phys. Rev. Lett. **33**, 1088 (1974).
[47] J. D. Jackson, *Classical Electrodynamics* (Wiley, New York, 1999).
[48] B. C. Carlson and G. S. Rushbrooke, Math. Proc. Cambridge. Philos. Soc. **46**, 626 (1950).
[49] W. P. Wolf and R. J. Birgeneau, Phys. Rev. **166**, 376 (1967).
[50] G. D. Scholes, Annu. Rev. Phys. Chem. **54**, 57 (2003).
[51] C. Crutchet, A. Franceschettti, A. Zunger, and G. D. Scholes, J. Phys. Chem. C **112**, 13336 (2008).
[52] R. Baer and E. Rabani, J. Chem. Phys. **128**, 184710 (2008).
[53] G. D. Scholes and D. L. Andrews, Phys. Rev. B **72**, 125331 (2005).
[54] G. Allan and C. Delerue, Phys. Rev. B **75**, 195311 (2007).
[55] Al. L. Efros, Phys. Rev. B **46**, 7448 (1992).
[56] P. Michler, A. Imamoglu, M. Mason, P. Carson, G. Strouse, and S. Buratto, Nature (London) **406**, 968 (2000).
[57] M. Dahan, T. Laurence, F. Pinaud, D. Chemla, A. Alivisatos, M. Sauer, and S. Weiss, Opt. Lett. **26**, 825 (2001).
[58] J. Zhang, X. Wang, and M. Xiao, Opt. Lett. **27**, 1253 (2002).

[59]G. Schlegel, J. Bohnenberger, I. Potapova, and A. Mews, Phys. Rev. Lett. **88**, 137401 (2002).
[60]X. Wang, L. Qu, J. Zhang, X. Peng, and M. Xiao, Nano Lett. **3**, 1103 (2003).
[61]Y. Matsumoto, R. Kanemoto, T. Itoh, S. Nakanishi, M. Ishikawa, and V. Biju, J. Phys. Chem. C **112**, 1345 (2007).
[62]B. Fisher, H. Eisler, N. Stott, and M. Bawendi, J. Phys. Chem. B **108**, 143 (2004).
[63]V. T. Forster, in *Modern Quantum Chemistry* (Academic, New York, 1965).
[64]E. A. Jares Erijman and T. M. Jovin, Nat. Biotechnol. **21**, 1387 (2003).
[65]F. Muller, S. Gotzinger, N. Gaponik, H. Weller, J. Mlynek, and O. Benson, J. Phys. Chem. B **108**, 14527 (2004).
[66]D. L. Dexter, J. Chem. Phys. **21**, 836 (1953).
[67]D. Beljonne, C. Curutchet, G. D. Scholes, and R. J. Silbey, J. Phys. Chem. B **113**, 6583 (2009).
[68]L. Guo, T. Krauss, C. Poitras, M. Lipson, X. Teng, and H. Yang, Appl. Phys. Lett. **89**, 061104 (2006).